Stopping cross sections for $N^{4+} \rightarrow H$ at low projectile velocity

Remigio Cabrera-Trujillo, John R. Sabin, Erik Deumens, and Yngve Öhrn
Quantum Theory Project, Departments of Physics and Chemistry, University of Florida, P.O. Box 118435, Gainesville, Florida 32611-8435

(Received 3 April 2002; published 13 August 2002)

We study the time-dependent dynamics of N^{4+} ions colliding with atomic hydrogen for projectile energies ranging from a fraction of an eV/amu up to 25 keV/amu using the electron-nuclear dynamics (END) formalism. The END theory obtains the electron-nuclear coupled equations of motion from the time-dependent variational principle employing a coherent state parametrization of the wave function. This approach leads to a simultaneous nonadiabatic dynamics of all the electrons and nuclei. We calculate and discuss dynamical trajectories, deflection functions, final charge states, differential cross sections, and energy loss. Quantum effects of the forward peak scattering are emphasized. Due to the strong interaction between the heavy ion and the hydrogen atom, a ''diffuse ion'' (*vide infra*) is formed, leading to acceleration or energy gain of the projectile. For the case of the electron transfer cross section, we found that it does not follow the Langevin-type cross section at low projectile energies as reported by other methods. Present results show good agreement with available experimental data.

DOI: 10.1103/PhysRevA.66.022706 PACS number(s): 34.50.Bw, 34.70.+e

I. INTRODUCTION

Recent research on energy transfer from swift ions to material targets seems to be dividing into two main groups: One that is concerned with developing a scheme which will reproduce experimental stopping powers and will predict stopping powers reliably for projectile velocities that have not yet been measured, and the other that is concerned with understanding the basic physical mechanisms occurring in the collision process. In the first group are included methods such as those of Ziegler [1], Paul [2], and Porter [3], which are based on fitting experimental data to an ansatz stopping function of some kind, as well as those methods which combine various theoretical constructs to form a description which fits experimental stopping data over a large projectile velocity range, such as that of Sigmund [4]. On the other hand, there are those schemes which apply purely quantum mechanical methods to the projectile-target system with the purpose of understanding the basic physics of the interaction, such as the work of Arista [5] and of Grande and Schiwietz [6,7].

A further distinction comes among groups in terms of the projectile velocity range which they find of interest. Low velocities, of the order of several tens of keV/amu down to eV/amu, are typically of greatest interest to the groups that apply first principles methods, as it is in this range that one finds the Bragg peak. This is the velocity regime where the greatest energy deposition occurs and where the projectile comes to rest. In addition, it is at low projectile velocities where the most interesting mechanisms for energy deposition occur.

Also, in recent years, it has been found that charge transfer is a major recombination process for various heavy charged ions in gases in a number of astrophysical phenomena; e.g., the general interstellar ''intercloud'' gas, ionized nebulas in the galaxy, the emission-line regions in quasars and Sayfert galaxies, and the interstellar gas near compact x-ray sources [8].

Traditionally, the calculations for charge transfer are performed in two steps. From electronic calculations, within the Born-Oppenheimer approximation, potential energy curves are obtained by means of variational, molecular orbital techniques. This information is used with a set of coupled equations that describe the scattering process in order to compute cross sections. Several approximations are utilized frequently to simplify this calculation, as, for example, assumption of straight trajectories, neglect of rotational coupling terms, or implementation of the well-known Landau-Zener treatment [9,10]. Furthermore, to ensure a proper induced dipole in the long range interaction, an *ad hoc* $-1/R^4$ potential may be introduced into the Hamiltonian, giving rise to a Langevin-type cross section [11] for orbiting collisions. Here R is the projectile-target internuclear distance. The validity of these approximations is, however, open to some question [12].

In this paper, we apply electron nuclear dynamics (END) [13], a fully quantum mechanical method for the electrons and semiclassical corrections for the nuclei, to examine the details of the collision between an N^{4+} ion projectile and a hydrogen atom target at projectile velocities from 0.1 eV up to several tens of keV, still well below the expected Bragg peak. In particular, due to the large mass and high charge of the projectile, application of perturbative models, as, for example, the Bethe theory [14], are not suitable, except at very high projectile energies. This low energy region also provides fertile ground for examining nonadiabatic effects in treating the electron-nuclei dynamics simultaneously, which constitutes the main difference between END and the methods described above. Such nonadiabatic effects are the principal focus of this study.

In Sec. II we give an overview of the END method, which we employ to perform the full dynamics of the collision. In Sec. III we give details of the calculations. In Sec. IV we present our results by reporting and analyzing the deflection function, direct differential cross section, electron transfer cross section, the energy loss and stopping cross section, and its acceptance angle analysis. Finally we conclude in Sec. V with a summary and discussion of further work.

II. END THEORY APPROACH

The END theory approximates the time-dependent Schrödinger equation by applying the time-dependent variational principle to the action for a dynamical system described by a nuclear and electronic wave function [15], resulting in a system of coupled, first order, ordinary differential equations. As the full details of the method, including detailed derivation and interpretation of the END equations, have been published elsewhere [13,15,16], we give here only an introductory account of the most salient features of the theory.

The minimal END theory, the level used in this work, consists of a single determinantal description of the electrons and a classical or narrow wave packet description of the nuclei. The END total wave function can be expressed as

$$|\psi\rangle = |z,R\rangle |R,P\rangle = |z\rangle |\phi\rangle, \tag{1}$$

where $|\phi\rangle = |R,P\rangle$ is the nuclear wave function, and R and P are $3N$ dimensional arrays of the positions and momenta of all N nuclei.

The electronic wave function is expressed as a complex, spin unrestricted, single determinant

$$|z\rangle = \det\{\chi_i(\mathbf{x}_j)\}, \tag{2}$$

where $\mathbf{x}_j$ is the three-dimensional position coordinate of electron j. The determinantal wave function is built from nonorthogonal dynamical spin orbitals

$$\chi_i = \phi_i + \sum_{j=N+1}^{K} \phi_j z_{ji}, \quad i = 1,2,\ldots,N, \tag{3}$$

which, in turn, are expressed in terms of a basis of atomic spin orbitals $\{\phi_i\}$ of rank K. The spin orbitals are formed from a Gaussian basis set centered on the average positions $\mathbf{R}$ of the participating atomic nuclei, which take into account the momenta of the electrons explicitly through electron translation factors (ETF). The particular form of parametrization of $|z\rangle$ with complex, time dependent coefficients z_{ji}, is due to Thouless [17], and is an example of a so-called generalized coherent state [18].

The application of the variational principle to the minimization of the action produces a set of dynamical equations that govern the time evolution of the dynamical variables $\{z,R,P\}$. The resulting END equations are expressed in matrix form as [13]

$$\begin{pmatrix} \mathbf{0} & -i\mathbf{C}^* & -i\mathbf{C}_\mathbf{R}^* & -i\mathbf{C}_\mathbf{P}^* \\ i\mathbf{C} & \mathbf{0} & i\mathbf{C}_\mathbf{R} & i\mathbf{C}_\mathbf{P} \\ i\mathbf{C}_\mathbf{R}^\dagger & -i\mathbf{C}_\mathbf{R}^\mathbf{T} & \mathbf{C}_{\mathbf{RR}} & -\mathbf{I}+\mathbf{C}_{\mathbf{RP}} \\ i\mathbf{C}_\mathbf{P}^\dagger & -i\mathbf{C}_\mathbf{P}^\mathbf{T} & \mathbf{I}+\mathbf{C}_{\mathbf{RP}} & \mathbf{C}_{\mathbf{PP}} \end{pmatrix} \times \begin{pmatrix} \dot{\mathbf{z}} \\ \dot{\mathbf{z}}^* \\ \dot{\mathbf{R}} \\ \dot{\mathbf{P}} \end{pmatrix} = \begin{pmatrix} \partial E/\partial \mathbf{z} \\ \partial E/\partial \mathbf{z}^* \\ \partial E/\partial \mathbf{R} \\ \partial E/\partial \mathbf{P} \end{pmatrix}, \tag{4}$$

where

$$E = \sum_k \frac{P_k^2}{2M_k} + \frac{\langle z,R|H_{el}|R,z\rangle}{\langle z,R|R,z\rangle} \tag{5}$$

is the total energy of the system and H_{el} is the electronic Hamiltonian which contains the nuclear-nuclear repulsion potential energy. The nonadiabatic coupling terms between the electronic and nuclear dynamics are expressed in terms of the elements of the dynamical metric on the left. In particular,

$$C = \frac{\partial^2 \ln S(z^*,R,P,z,R',P')}{\partial z^* \partial z}\Big|_{R'=R,P=P'}, \tag{6}$$

$$C_R = \frac{\partial^2 \ln S(z^*,R,P,z,R',P')}{\partial z^* \partial R'}\Big|_{R'=R,P=P'}, \tag{7}$$

$$C_{RR} = -2\,\mathrm{Im}\frac{\partial^2 \ln S(z^*,R,P,z,R',P')}{\partial R \partial R'}\Big|_{R'=R,P=P'}, \tag{8}$$

with similar definitions for C_{RP}, C_P, and C_{PP}. These coupling terms are defined in terms of the overlap $S(z^*,R,P,z,R',P') = \langle z,R',P'|z,R,P\rangle$ of the determinantal states of two different nuclear configurations. When the effects of the electron translation factors are neglected, this set of equations reduces to a simple form [19] corresponding to purely classical equations of motion for the nuclear positions.

III. DETAILS OF CALCULATION

For each projectile trajectory, the target was placed at the origin of a Cartesian laboratory coordinate system with the initial projectile velocity parallel to the x axis and directed toward the target with an impact parameter b, measured along the z axis. The projectile was started 30 a.u. from the target and the trajectory was followed until the projectile was 30 a.u. past the target, or until there were no longer changes in the energy or charge of the projectile.

The basis functions used for the atomic orbital expansion for the N^{4+} and H were derived from those of Dunning [20] and were centered on the moving nuclei. The combination of these basis sets on the determinant describing the total system (supermolecule description), as required by Eq. (2), produces a set of 20 different accessible electronic states. Initially the projectile and target are in their SCF ground state, as generated within the Hartree-Fock model. Of the 20 electronic states, five lie in the lower part of the continuum.

The initial electronic configuration for N^{4+} is $1s^2 2s$. For the atomic hydrogen target, its initial electronic configuration is $1s$. Thus we need to take into account the two possibilities for the total spin states for the supermolecule, i.e., singlet or triplet [(α,β) spin, or (α,α) spin] states. All our results are averaged over these two configurations.

Since the majority of the electronic capture for the N^{4+} ion occurs in its $3s,3p$ states, we have to ensure that our basis set gives a proper description of these states by incorporating diffuse orbitals in the N^{4+} ion basis set. A diffuse

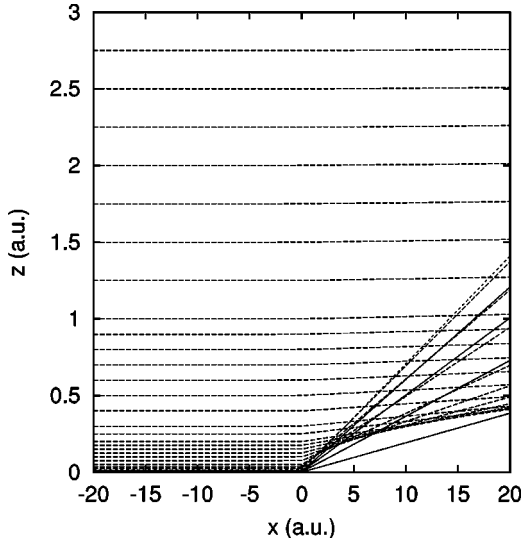

FIG. 1. N^{4+} projectile trajectory when colliding with atomic neutral hydrogen targets for $E_p = 5.0$ keV/amu for various impact parameters.

orbital is one with a small exponent such that the electron position expectation value, $\langle r \rangle$, is large. This type of orbitals are suitable to describe Rydberg-type orbitals.

The solutions of Eq. (4) for the positions, momentum, and wave function coefficients were performed by our ENDyne code [21].

IV. RESULTS

A. Deflection function

Once we have calculated the dynamics of the collision, we obtain the final electronic wave function, as well as the final nuclear momentum and position. In Fig. 1 we show a representation set of trajectories in the scattering plane for the N^{4+} ion when colliding with neutral H for a projectile energy of 5.0 keV/amu at various impact parameters. We note that for small impact parameters, the deflection of the projectile shows a repulsive envelope. We note that in none of the trajectories calculated in this study were orbiting trajectories observed.

At the terminus of each trajectory, we obtain the final momentum of the projectile, $\hbar \mathbf{k}_f(E_p,b)$, which defines the deflection function for the projectile when projected on the initial momentum, $\hbar \mathbf{k}_i$, i.e., $\Theta(E_p,b) = \arccos[\mathbf{k}_f(E_p,b) \cdot \mathbf{k}_i / k_f(E_p,b) k_i]$ for each impact parameter b, which describes the dynamical interaction between projectile and target. The scattering angle is defined as the absolute value of the deflection function for the projectile, i.e., $\theta = |\Theta(E_p,b)|$.

In Fig. 2 we show the deflection function $\Theta(E_p,b)$ for N^{4+} colliding with atomic hydrogen as a function of the projectile energy and impact parameter. From these results, we note that for low projectile energies, the deflection function becomes broader, indicating that large impact parameter collisions suffer significant deflections as the interaction time lengthens. This longer collision time is reflected in the electronic structure of the colliding system, modifying the interaction potential. Also, we observe the shell structure of the N^{4+} at low projectile energies, suggesting an exchange of electrons, and thus, a dynamical potential. Furthermore, we observe a ridge for the rainbow angle that extends towards the low energy region and large impact parameter, showing again the long range interaction of the collision for the low energy region. Also, the impact parameter b_r, corresponding to the rainbow angle θ_r, becomes smaller, closer to the atomic nucleus target, as the projectile energy increases. This indicates that for high energies, the heavy N^{4+} ion penetrates the electron cloud of the H target. In addition, we present the contour lines for some scattering angles; in particular, note the contour line for no deflection, i.e., the glory angle for $b_g \sim 9.0$. For impact parameter $b > b_g$, the projectile is attracted by the target, due to charge induced dipole interaction. This long range interaction will populate electronically some low lying excited states, with some inner shells empty as we discuss in Sec. IV C. These effects are nonadiabatic and will contribute to the diffuse electronic structure of the N^{3+} resulting from the dynamical interaction. We will discuss these effects in more detail in the next sections.

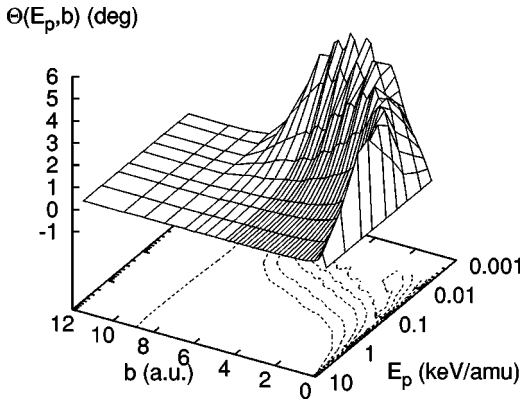

FIG. 2. Scattering angle in the laboratory frame, $\Theta(b,E_p)$, as a function of the projectile impact parameter and incident energy.

B. Direct differential cross section

From the deflection function presented in the previous section, we calculate the differential cross section. As we note in Fig. 2, there can be several different trajectories (two different impact parameters) that produce the same scattering angle. Thus two different trajectories for which the N^{4+} ion will arrive at a particular point in the detector, and therefore their nuclear wave functions will interfere quantum mechanically. This analysis requires the implementation of semiclassical corrections to the narrow nuclear width approximation (classical nuclei).

We have implemented semiclassical corrections to the END method via the Schiff approximation [22] for small scattering angles. The direct differential cross section in the Schiff approximation within the END approximation is given by [23]

$$\frac{d\sigma}{d\Omega} = \frac{k_f}{k_i} |f(\theta,\varphi)|^2 \tag{9}$$

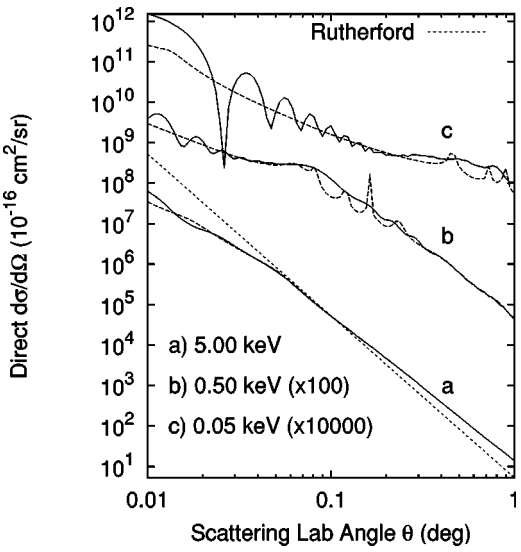

FIG. 3. Direct differential cross section for N^{4+} ions colliding at 0.05, 0.5, and 5.0 keV/amu with atomic hydrogen, as obtained by the END method (solid line). The long-dashed line is the classical results from Eq. (11) and the short-dashed line is the Rutherford cross section.

with the scattering amplitude

$$f(\theta,\varphi)=ik_i\int_0^\infty J_0(qb)(e^{2i\delta(b)}-1)b\,db. \tag{10}$$

Here, $J_0(x)$ is the Bessel function of zero order, $q=|\mathbf{k}_f-\mathbf{k}_i|$ is the momentum transfer, which depends on the scattering angle θ, and $\delta(b)$ is the semiclassical phase shift, which is given in terms of the deflection function as $\Theta(b)=d\delta(b)/2k_i db$.

Using the deflection function from Fig. 2 in Eq. (9), we obtain the direct differential cross section for N^{4+} ions colliding with neutral hydrogen for projectile energies of 0.05, 0.5, and 5.0 keV/amu. These results are shown in Fig. 3. Note that for high energies, the direct differential cross section shows typical Rutherford scattering, characteristic of a heavy ion scattering process. However, for low projectile energies, and as discussed previously, the long collision time and the changing electronic structure of the ion modifies dynamically the interaction potential producing the rainbow angle, and therefore interference in the direct differential cross section, as shown in Fig. 3. Note that for low energies, the direct differential cross section shows a plateau in the scattering angle. From Fig. 2 we see that for the corresponding angular range as for the plateau observed in Fig. 3, the deflection function shows a slope which is almost inversely proportional to the sine of the scattering angle. In other words, the classical direct differential cross section

$$\frac{d\sigma}{d\Omega}=\frac{b}{\sin\theta\left|\frac{d\Theta}{db}\right|} \tag{11}$$

will be constant as a function of the scattering angle, when $|db/d\Theta|\sim\sin\theta$. Furthermore, we show in the same figure, the classical direct differential cross section, as given by Eq. (11), for comparison to the Schiff approximation, which takes into account the quantum effects of the forward scattering.

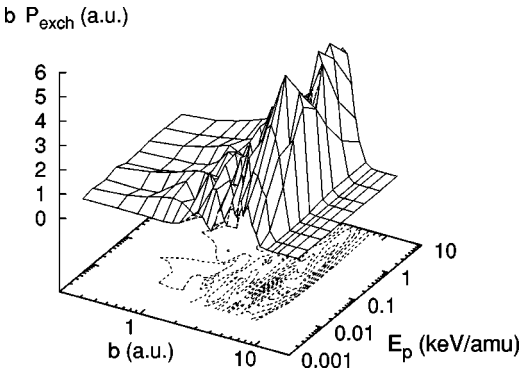

FIG. 4. Charge exchange probability times the impact parameter, bP_{exch}, as a function of the impact parameter and projectile energy.

C. Electron transfer cross section

Due to the interaction of the projectile with the target, the projectile might capture or lose electrons. From the evolving molecular state wave function, we can determine the number of electrons associated with a projectile and thus determine the probability of electron capture or loss. For this, we use the Mulliken population analysis [24]. From Eqs. (2) and (3), the total number of electrons in the system is [19]

$$N=\sum_{\nu,\mu}P_{\nu\mu}\Delta_{\mu\nu}=\sum_{\nu}(\mathbf{P}\Delta)_{\nu\nu}=\mathrm{Tr}(\mathbf{P}\Delta), \tag{12}$$

where $P_{\nu\mu}=\Sigma_i z_{i\nu}z_{i\mu}$ and $\Delta_{\mu\nu}$ is the atomic orbital overlap matrix. It is possible to interpret $(\mathbf{P}\Delta)_{\mu\mu}$ as the number of electrons to be associated with the basis function u_μ. Thus $n_A=\Sigma_{\mu\in A}(\mathbf{P}\Delta)_{\mu\mu}$ is the number of electrons associated with nuclei A. Knowing the initial number of projectile electrons allows one to calculate the probability for electron capture or loss.

From the probability for charge exchange, the charge exchange cross section can be obtained from

$$\sigma_{exch}(E_p)=2\pi\int_0^\infty P_{exch}(b,E_p)\,b\,db. \tag{13}$$

Before discussing the results for the charge exchange cross section, let us analyze our results for the integrand of Eq. (13). First let us note that the main electron transfer process is electron capture. Projectile electron loss has a low probability for the projectile energies of interest in this work. For larger projectile energies it becomes of importance and requires a description using proper continuum states.

In Fig. 4 we show the charge exchange probability times the impact parameter as a function of the impact parameter and of the projectile energy. The largest contribution to the electron capture cross section comes from impact parameters in the range $b\sim 6$ to 7 a.u. for all the energies. This confirms

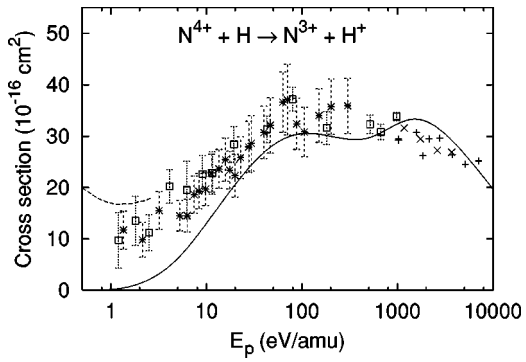

FIG. 5. Total charge exchange cross section for N^{4+} colliding with atomic H as a function of the projectile energy. For comparison, we also show the theoretical coupled channel results (dashed line) from Feickert [11]. The experimental data are from □: Huq *et al.* [27]; +: Crandall *et al.* [28]; ×: Seim *et al.* [29]; and *: Folkerts *et al.* [25].

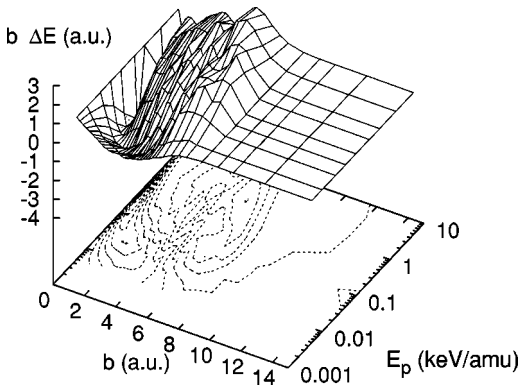

FIG. 6. Kinetic energy loss ΔE times the impact parameter b as a function of the projectile impact parameter and incident energy for the N^{4+} ion projectile when colliding with atomic hydrogen.

our previous discussion concerning the long range nature of the collision. Also, this means that the N^{4+} ion captures the hydrogen electron in a shell approximately 6 to 7 a.u. from its center, thus forming what we denote as a "diffuse ion" with the three core electrons having configuration $1s^2 2s$ and the captured electron having highest probability in the $3s,3p$ orbitals [25]. The resulting object is similar to a "hollow atom," which is defined as a "*multiple excited (dynamically neutral) atom with most or all of its electrons in outer energy levels, while inner shells remain empty*" [26]. The difference with our diffuse ion is in the neutral state of the hollow atom and empty inner shells. Furthermore, there are two maxima in the charge exchange probability as a function of the projectile energy. The first occurs around $E_p \sim 0.1$ keV/amu and the second one around $E_p \sim 2$ keV/amu.

From the charge exchange probability in Eq. (13), we obtain the total charge exchange cross section, shown in Fig. 5. In the same figure we present, for comparison, some experimental results [25,27–29]. From our results, we observe a similar trend to that shown in Fig. 4, i.e., the total cross section shows two maxima at energies around 0.1 and 2.0 keV/amu, respectively. We also note that the calculated charge exchange cross section vanishes for low energy projectiles. This seems to agree with the experimental trend, but unfortunately we were not able to find more experiments in the lower region of the projectile energy. For completeness, we also show the results obtained by Feickert *et al.* [11] by means of a coupled channel theory and a fitted charge exchange potential. Their results predict that for lower energies, the charge exchange cross section will increase as the projectile energy decreases; the well known Langevin-type cross section for orbiting. As we explained in the Introduction, the reason is the introduction of an attractive polarization potential (induced dipole) between the neutral H and the N^{4+} ion for large distances. But when the electron-nuclear dynamics (nonadiabatic effects) are taken into account, the charge transfer is not enhanced for the low projectile energies, where the momentum transfer is low such that there is not enough energy for electron transfer, but just enough for electron excitation and nuclear displacement as we discuss in the next section. This also elucidates the reason why the results of Feickert [11] predict an order of magnitude larger reaction rate for the collision.

In general, our results are in fair agreement with the experimental data for the available experimental data region, and thus provide confidence that we capture the essence of the correct physical description of the collision. In the next section we proceed to calculate the projectile energy loss and stopping cross section.

D. Energy loss and stopping power

Our main interest in the implementation of the END approach is to understand the process of energy loss suffered by the projectile and by which modes energy is transfered to the target. The stopping power, or energy loss per unit length for a projectile, is given by

$$S(E_p) = -\frac{1}{n_2}\frac{dE}{dx} = -\int \Delta E(E_p,\Omega)\frac{d\sigma}{d\Omega}d\Omega, \qquad (14)$$

where n_2 is the number of target scattering center per unit volume, ΔE is the kinetic energy loss of the projectile, and $d\sigma/d\Omega$ is the direct differential cross section. By using the deflection function, $\Theta(b)$, we can transform the integral to the impact parameter representation, thus

$$S(E_p) = -\int b\,\Delta E(E_p,b)db\,d\varphi. \qquad (15)$$

In Fig. 6 we show the kinetic energy loss, $\Delta E = K_f - K_i$, times the impact parameter, to be used in Eqs. (14) or (15), for an N^{4+} ion projectile colliding with neutral atomic hydrogen, as a function of the impact parameter and projectile energy, and in the absence of Auger and photon emission. From this figure, we observe two important differences with respect to the usual shape of energy loss curves for protons or α particles [19,30]. First, there is a maximum and a minimum in the kinetic energy loss. The maximum, which represents a gain in the energy of the projectile, occurs for projectile energies from 0.1 to 10 keV and large impact parameters from 3 to 8 a.u. This is precisely the same region for which the ion projectile experiences the largest electron

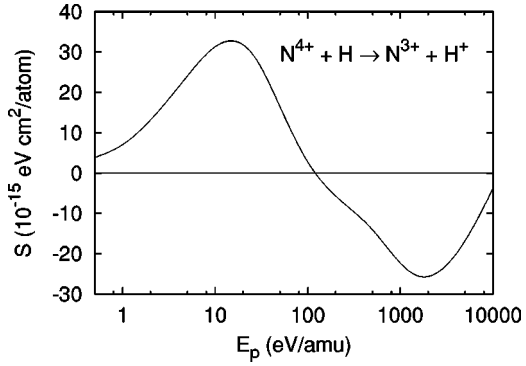

FIG. 7. Stopping cross section as a function of the projectile energy for N^{4+} ions colliding with neutral hydrogen.

capture. Thus, by energy conservation, the projectile is accelerated. The minimum, which represents the greatest energy loss of the projectile, is more broad and occurs in the small impact parameter region, widening at low projectile energies. A detailed study of projectile acceleration effects is under preparation [31]. The second characteristic is that the nuclear and electronic energy loss maxima are merged in the results, when in the typical case (see Refs. [19,30]) the two maxima were easily distinguishable. This is due to the large mass of the ion projectile and the strong interaction due to the high charge in the ion.

By integrating the previous results over impact parameter, we obtain the stopping cross section, as shown in Fig. 7. As anticipated in the previous discussion, we note two extrema in the stopping cross section. The first corresponds to the energy loss for $E_p \sim 0.01$ keV/amu, and the second corresponds to the energy gained by the projectile around $E_p \sim 2$ keV/amu.

The fact that the collision is exoergic allows a detailed analysis of the excited states involved in the electron transfer via an energy gain spectroscopy analysis. In our case, we can relate it to the excited states and the scattering angle. The exoergecity of the collision arises when electron transfer is involved. Initially the electron of the H atom has a binding energy of 13.6 eV. When it is captured into the $N^{4+}(3s,3p)$ state with a binding energy of 59.3 eV, there is an extra energy of ~ 45 eV. This is the reason for the accelerated projectile. A more detailed work is in progress and will be reported elsewhere.

In order to have a deeper understanding of the total stopping cross section for the heavy N ion colliding with atomic hydrogen, we require an analysis of the different charge state channels, i.e., N^{+q}, with $q=0,1,\ldots,7$. This is work in progress and will be reported elsewhere. In the next section we analyze the angular scattering dependence of the stopping and charge exchange cross sections.

E. Acceptance angle analysis

In Eq. (14), the integration is performed over all scattering angles $0 \leq \Omega \leq 4\pi$, including the backward direction, or from Eq. (15), integration is over all impact parameters. However, in an experiment, the geometry of the detector restricts the range of scattering angles through which the particles can be detected. We assume an experimental geometry such that the scattered particle with a scattering angle less than θ_a reaches the detector. In the binary collision approximation, it is equivalent to restricting the integration of Eq. (14) to a scattering angle θ_a, the acceptance angle, or to a selected group of impact parameters defined by the deflection function. This is the impact parameter selection of Semrad [32]. Thus, when $\theta_a \rightarrow \pi$, we obtain the total stopping cross section. Analysis of the acceptance angle dependent stopping cross section allows a more precise understanding of the energy loss process.

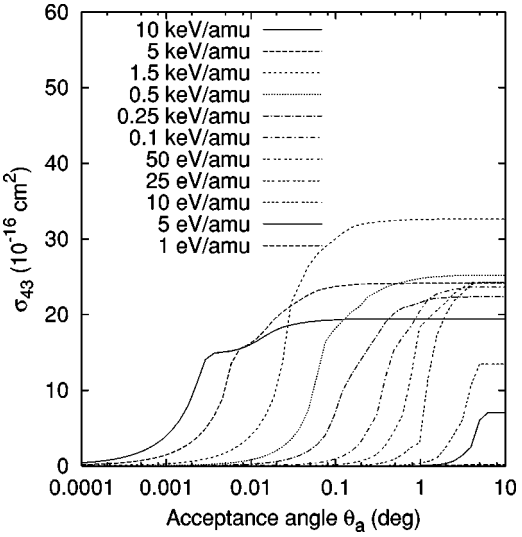

FIG. 8. Acceptance angle vs charge exchange cross section for the reaction $N^{4+}+H \rightarrow N^{3+}+H^+$ as a function of the acceptance angle of the exit window θ_a for several projectile energies.

In Fig. 8 we show the results of integrating Eq. (14) up to an angle θ_a for the charge exchange cross section. We note that for high projectile energies, the charge exchange cross section saturates at very small acceptance angles, thus justifying the rectilinear trajectory assumption of several other models at high energy [7]. However, for low projectile ener-

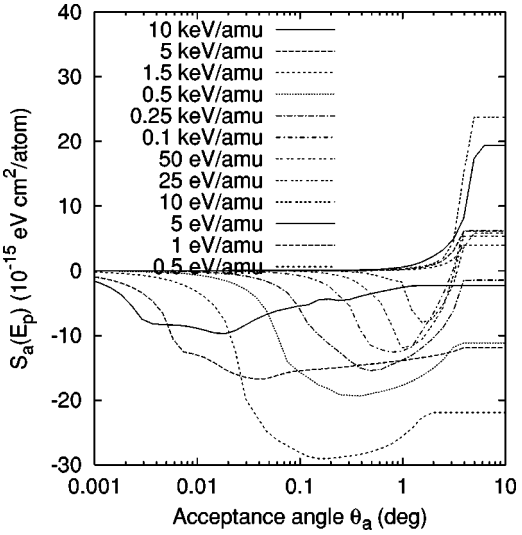

FIG. 9. The same as Fig. 8 but for the stopping cross section.

gies, we note that, in order to saturate the charge exchange cross section, larger acceptance angles are required, and thus a breakdown of the rectilinear assumption occurs.

In Fig. 9 we show the acceptance angle dependent stopping cross section, as discussed previously. Here we observe some interesting behavior. For small acceptance angles we observe that the particles detected will be accelerated, i.e., will gain energy for large projectile energies, in agreement with our previous discussion. This happens up to an acceptance angle of around $\theta_a \sim 2°$. For low projectiles energies, where we have seen that larger angles become more important, the energy loss is still negative for small acceptance angles, but then at large angles, the particles that lose energy start to be detected. Thus reaching saturation for energy loss at large acceptance angles.

From the previous discussion, in an experimental setup for a heavy ion projectile colliding with light targets, these effects we have discussed should be observable.

V. SUMMARY

We have employed the electron-nuclear dynamics approach to the study of the collision of the heavy and highly charge ion N^{4+} with neutral atomic hydrogen targets for projectile energies ranging from a fraction of an eV/amu up to 10 keV/amu. The effects and processes which take place in this collision are different from those of standard proton and α-particle energy loss studies. Effects such as ''diffuse ion'' formation in the heavy ion projectile, energy loss and energy gain in the projectile at different projectile energies, and impact parameters take place. At low projectile energies, the electron transfer cross section does not follow the typical Langevin-type cross section characteristic of long range interactions as reported by other models. The analysis of the acceptance angle dependence on the stopping cross section shows that for small scattering angles, the projectile loses energy. Thus heavy ions studies in the intermediate projectile energy range seem to be an interesting and promising field in collision and energy loss studies.

ACKNOWLEDGMENTS

This work was supported in part by CONACyT-Mexico to R.C.T., by NSF (Grant No. CHE-9732902 to N.Y.O. and CHE-9974385 to J.R.S.), and by ONR (Grant N0014-00-1-0197 to N.Y.O. and N00014-96-1-0707 to J.R.S.), and by the IBM SUR program for 1999.

[1] J.F. Ziegler, J.P. Biersack, and U. Littmark, *The Stopping and Range of Ions in Solids* (Pergamon, New York, 1985).
[2] H. Paul and A. Schinner, Nucl. Instrum. Methods Phys. Res. B **179**, 299 (2001).
[3] L.E. Porter, E. Rauhala, and J. Räisänen, Phys. Rev. B **49**, 11543 (1994).
[4] P. Sigmund and A. Schinner, Eur. Phys. J.D **12**, 425 (2001).
[5] N.R. Arista, Nucl. Instrum. Methods Phys. Res. B **164-165**, 108 (2000).
[6] G. Schiwietz, Phys. Rev. A **42**, 296 (1990).
[7] P.L. Grande and G. Schiwietz, Phys. Rev. A **44**, 2984 (1991).
[8] A. Dalgarno and S.E. Buttler, Comments At. Mol. Phys. **7**, 129 (1978).
[9] A. Dalgarno, C. Bottcher, and G.A. Victor, Chem. Phys. Lett. **7**, 265 (1970).
[10] R. McCarroll and P. Valiron, Astron. Astrophys. **53**, 83 (1976).
[11] C.A. Feickert, R.J. Blint, G.T. Surrat, and W.D. Watson, Astrophys. J. **286**, 371 (1984).
[12] W.D. Watson and R.B. Christensen, Astrophys. J. **231**, 627 (1979).
[13] E. Deumens, A. Diz, R. Longo, and Y. Öhrn, Rev. Mod. Phys. **66**, 917 (1994).
[14] H.A. Bethe, Ann. Phys. (Leipzig) **5**, 325 (1930).
[15] Y. Öhrn, E. Deumens, A. Diz, R. Longo, J. Oreiro, and H. Taylor, *Time-Dependent Quantum Molecular Dynamics* (Plenum, New York, 1992).
[16] E. Deumens, A. Diz, H. Taylor, and Y. Öhrn, J. Chem. Phys. **96**, 6820 (1992).
[17] D.J. Thouless, Nucl. Phys. **21**, 225 (1960).
[18] J.R. Klauder and B.S. Skagerstman, *Coherent States, Applications in Physics and Mathematical Physics* (World Scientific, Singapore, 1985).
[19] R. Cabrera-Trujillo, E. Deumens, Y. Öhrn, and J.R. Sabin, Nucl. Instrum. Methods Phys. Res. B **168**, 484 (2000).
[20] T.H. Dunning, J. Chem. Phys. **90**, 1007 (1989).
[21] E. Deumens, T. Helgaker, A. Diz, H. Taylor, J. Oreiro, J.A. Morales, and R. Longo, ENDyne version 2.7 Software for Electron Nuclear Dynamics, Quantum Theory Project, University of Florida, 1998.
[22] L.I. Schiff, Phys. Rev. **103**, 443 (1956).
[23] R. Cabrera-Trujillo, J.R. Sabin, Y. Öhrn, and E. Deumens, Phys. Rev. A **61**, 032719 (2000).
[24] R.S. Mulliken, J. Chem. Phys. **36**, 3428 (1962).
[25] L. Folkerts, M.A. Haque, C.C. Havener, N. Shimakura, and M. Kimura, Phys. Rev. A **51**, 3685 (1995).
[26] H. Winter and F. Aumayr, J. Phys. B **32**, R39 (1999).
[27] M.S. Huq, C.C. Havener, and R.A. Phaneuf, Phys. Rev. A **40**, 1811 (1989).
[28] D.H. Crandall, R.A. Phaneuf, and F.W. Meyer, Phys. Rev. A **19**, 504 (1979).
[29] W. Seim, A. Müller, I. Wirkner-Bott, and E. Salzborn, J. Phys. B **14**, 3475 (1981).
[30] R. Cabrera-Trujillo, J.R. Sabin, E. Deumens, and Y. Öhrn, in *Application of Accelerators in Research and Industry: Sixteenth International Conference*, Denton, TX, 2000 (AIP Melville, NY, 2001), p. 3.
[31] R. Cabrera-Trujillo, J.R. Sabin, Y. Öhrn, and E. Deumens (unpublished).
[32] D. Semrad, M. Bergsmann, P. Bauer, R. Diez-Muiño, and S.A. Arnau, Nucl. Instrum. Methods Phys. Res. B **164-165**, 284 (2000).